The effect of different evapotranspiration methods on portraying soil water dynamics and ET partitioning in a semi-arid environment in Northwest China

Lianyu Yu[1, 2], Yijian Zeng[3], Zhongbo Su[3], Huanjie Cai[1, 2], Zhen Zheng[1, 2]

1. Key Laboratory of Agricultural Soil and Water Engineering in Arid Area of Ministry of Education, Northwest Agriculture and Forestry University, Yangling, China.

2. Institute of Water Saving Agriculture in Arid Regions of China (IWSA), Northwest Agriculture and Forestry University, Yangling, China.

3. Faculty of Geo-Information Science and Earth Observation, University of Twente, Enschede, Netherlands.

Correspondence to: H. Cai (caihj@nwsuaf.edu.cn)

Abstract

Different methods for assessing evapotranspiration (ET) can significantly affect the performance of land surface models in portraying soil water dynamics and ET partitioning. An accurate understanding of the impact a method has is crucial in determining the effectiveness of an irrigation scheme. Two evapotranspiration (ET) methods are discussed: one, based on reference crop evapotranspiration (ET_0) theory, uses leaf area index (LAI) for partitioning into soil evaporation and transpiration and is denoted as the ET_{ind} method; the other is a one-step calculation of actual soil evaporation and potential transpiration by incorporating canopy minimum resistance and actual soil resistance into the Penman-Monteith model, and is denoted as the ET_{dir} method. In this study, a soil water model, considering the coupled transfer of water, vapor, and heat in the soil, was used to investigate how different ET methods could

affect the calculation of the soil water dynamics and ET partitioning in a crop field. Results indicate that for two different ET methods this model varied concerning the simulation of soil water content and crop evapotranspiration components, but the simulation of soil temperature agreed well with lysimeter observations. Considering aerodynamic and surface resistance terms improved the ET_{dir} method regarding simulating soil evaporation, especially after irrigation. Furthermore, the results of different crop growth scenarios indicate that the uncertainty in LAI played an important role in estimating the relative transpiration and evaporation fraction. The impact of maximum rooting depth and root growth rate on calculating ET components might increase in drying soil. The influence of maximum rooting depth was larger late in the growing season, while the influence of root growth rate dominated early in the growing season.

1 Introduction

Soil water movement forms the central physical process in the land surface models (LSMs), interacting with surface infiltration, evaporation, root extraction and underground water recharge. Accurate description of this process is necessary for the application of LSMs to achieve efficient and optimum water resources management. While it has been widely accepted that water vapor and heat transport should be incorporated in a soil water model, especially in arid or semi-arid environments (Bittelli et al., 2008; Saito et al., 2006; Zeng et al., 2009a, b, 2011a, b), it is still not clear how these factors affect soil water dynamics in crop fields.

ET plays a critical role in the process of soil water movement, as it controls the water distribution of surface and root zone soil layers through soil evaporation and transpiration. A common procedure to estimate ET is the so-called indirect ET method (ET_{ind}), which transfers the reference crop evapotranspiration (ET_0) into actual crop evapotranspiration (ET_c) using a simple multiplicative crop factor. Recent theoretical developments allow the adoption of a more robust Penman-Monteith (PM) equation description of ET. The direct ET method (ET_{dir}) is a one-step calculation procedure,

which expresses the stomatal and aerodynamic controls in terms of various resistances in the PM equation. Independent from land surface models (LSMs), much effort has been made to compare the performances of different approaches to estimate ET (Federer et al., 1996; Stannard, 1993). The performance of different ET equations varies with the characteristics of land cover and climate (Shuttleworth and Wallace, 2009; Zhou et al., 2007). Ershadi et al. (2015) highlight the need for guidance in selecting the appropriate ET method for use in a specific region.

Further evaluation confirms that different ET methods can significantly affect the performance of LSMs (Anothai et al., 2013; Chen et al., 2013; Federer et al., 1996; Kemp et al., 1997; Mastrocicco et al., 2010). Vörösmarty et al. (1998) made a comparison between reference surface and surface cover-dependent potential ET (PETr and PETs, respectively) methods in a global-scale water balance model (WBM) and concluded that WBM simulations were highly sensitive to the PET method used and that the PETs method would produce quite reasonable estimates of actual ET over a broad geographic domain. Recent assessment of the HYDRUS-1D model with different ET methods indicated that using the PM equation gave a better model performance in simulating soil water content (Mastrocicco et al., 2010). However, most of this research only evaluates model performance for an individual variable (e.g. soil water content or ET) or neglects the heat or vapor transport effect (Anothai et al., 2013; Kemp et al., 1997; Vörösmarty et al., 1998).

In addition, uncertainties of crop growth parameters are not fully tested despite having a significant influence on model performance (Federer et al., 2003). Previous studies generally based conclusions on the combined analysis of the entire growing season (Padilla et al., 2011). However, these results could be inappropriate to some extent. Unlike soil properties, crop growth parameters are significantly affected by a changing environment during the growing season (Teuling et al., 2006). A roughly seasonal assessment would conceal the crop modulating mechanism associated with a changing environment.

The objectives of this study are twofold: i) comparing with observations of obtained

through a lysimeter experiment, we investigate how different methods for measuring ET will affect the assessment of soil water dynamics in a crop field located in a semi-arid environment in Northwest China, based on a coupled model considering transfer of water, vapor and heat in the soil; ii) with the calibrated coupled model, a sensitivity analysis is conducted to explore the influence of crop growth parameters on the ET partitioning. In the following section, the field experiment, data collection and the numerical models will be introduced. The results are discussed in section 3. The summary and conclusions are presented in section 4.

2 Materials and methods

2.1 Field experiment

The lysimeter experiment was conducted at the Yangling Irrigation Experiment Station located in Northwest China (34°17′N, 108°04′E, at an elevation of 521m a.s.l.). The experimental site is located in a semi-arid to sub-humid climatic region with a mean annual precipitation of 630mm and a mean annual air temperature of 12.9 ℃. The soil at the location is silt clay loam with a field capacity of 23.5% and bulk density of 1.35 g cm^{-3}. Groundwater level is at least 50m below the soil surface (Kang et al., 2001), thus the capillary rise from groundwater can be neglected in the current study.

The lysimeter is made of steel and is 3 by 2.2 by 3m (length, width and depth, respectively) in size. It contains a filter layer, a weighing facility and a drainage system for measuring the amount of deep percolation at the bottom of the lysimeter. Weight data generated by the weighing system and drainage system were stored in the datalogger. The data collector was programmed to record weight readings hourly with a precision of 139g (i.e. 0.021mm of water) for the weighing system and 1g for the drainage system, respectively. In order to be able to apply irrigation water, the steel wall rises 5cm above the ground surface. A detailed drawing of the lysimeter is presented in **Fig.1**. A mobile rainproof shelter was installed above the lysimeter to control precipitation. Summer maize was sown 23 June 2013 and harvested 2 October

2013 with a plant population of 40 plants within an area of 6.6 m^2. Irrigation was applied when the soil water content dropped below a pre-set limit (i.e. 60% of the field capacity). The level of irrigation was set to replace crop water consumed since the previous irrigation, as measured by the lysimeter. Two supplemental irrigations were applied in the early growing season (DOY 178 and 184) to ensure uniform growth of the summer maize.

2.2 Data collection

Soil moisture and temperature were measured using the pre-calibrated sensors, which were installed at depths of 20, 40, 60, 80, 100, 200, 225, and 250 cm. The type of soil moisture sensors used was ThetaProbe ML2x (Delta-T Devices Ltd, Cambridge, UK), which specifies a range of 0 to 100% volumetric water content, and 1% and 2% precision for temperatures between 0-40°C and 40-70°C, respectively. Soil temperature was measured by QYWD100, made by Xi'An QingYuan Measurement & Control Technology Co. Ltd. , with a range from -30 to 50°C; and a higher than 1°C accuracy. Hourly measurements were taken throughout the growing season. Considering the possibility of damage caused by tillage and other agricultural management, soil moisture and temperature sensors were not placed in the top soil layers. Top soil water content was measured using the gravimetric method weekly. Crop ET was determined using the lysimeter weighting system (with an accuracy of 0.021 mm). The ET measurements were taken hourly and summed to daily values during the growing season. The micro-lysimeter, with a diameter of 12cm, a depth of 20cm, and containing a small isolated volume of bare soil, was placed between two crop rows (**Fig.1**). Soil evaporation (E) was measured by weighing the micro-lysimeter at 8:00 a.m. daily. After significant precipitation or irrigation, we replaced the soil in the micro-lysimeter to keep the soil moisture in the micro-lysimeter similar to that of surrounding field. Changes in the weight of the micro-lysimeter were assumed to be equivalent to the amount of water evaporated from the soil surface (Boast and Robertson, 1982). The source of error inherent in the micro-lysimeter method was discussed and some recommendations for the use of the

micro-lysimeter were made in our study area (Kang et al., 2003; Wang et al., 2007).

Meteorological data were obtained from a standard weather station located inside the experimental site. The data included daily maximum and minimum air temperature, air humidity, daily precipitation, hours of sun, and wind speed at 10m height. Hourly values of air temperature, air humidity and wind speed were generated from daily measurements using a trigonometric function, of which a detailed description can be found in Saito et al. (2006).

Leaf stomatal conductance was measured using portable photosynthesis equipment (LI-6400, Li-Cor, USA) a few days after irrigation. Measurements were taken from three functional leaves at time intervals between 10:00-14:00 local time, when the stomatal conductance of summer maize reached its peak and remained steady (Zhang et al., 2011). Leaf area and plant height were measured, based on the average of at least 3 plant samples, at intervals of 7-10 days starting at 14 days after planting. The crop stages or phenology were assessed according the recommendations by Allen et al. (1998). Dates for each crop development phase are shown in **Table 1**.

2.3 Numerical Model

The STEMMUS (Simultaneous Transfer of Energy, Mass and Momentum in Unsaturated Soil) model was used to simulate coupled liquid water, water vapor and heat flow in unsaturated soil. In order to use STEMMUS for the lysimeter experiment, a macroscopic root water uptake module was incorporated into the STEMMUS model.

2.3.1 STEMMUS

In STEMMUS, the extended version of Richards (1931) equation with modifications made by Milly (1982) was numerically solved to consider the vertical interactive process between atmosphere and soil. The governing equation of the liquid and vapor flow can be expressed as:

$$\frac{\partial}{\partial t}\left(\rho_L\theta_L+\rho_V\theta_V\right)=-\frac{\partial q_L}{\partial z}-\frac{\partial q_V}{\partial z}-S \quad (1)$$

where ρ_L and ρ_V (kg m^{-3}) are the density of liquid water and water vapor, respectively; $\theta_L$and θ_V (m^3 m^{-3}) are the volumetric water content (liquid and vapor, respectively); z (m) is the vertical space coordinate; q_L and q_V (kg m^{-2} s^{-1}) are the soil water fluxes of liquid water and water vapor (positive upwards), respectively; and S (s^{-1}) is the sink term for the root water extraction.

The liquid water flux, separated into isothermal q_{Lh} (pressure head driven) and thermal q_{LT} (temperature driven), is described as:

$$q_L=q_{Lh}+q_{LT}=-\rho_L K_{Lh}\left(\frac{\partial h}{\partial z}+1\right)-\rho_L K_{LT}\frac{\partial T}{\partial z} \quad (2)$$

where K_{Lh} (m s^{-1}) and K_{LT} (m^2 s^{-1} °C^{-1}) are the isothermal and thermal hydraulic conductivities, respectively; h (m) is the pressure head; and T (°C) is the soil temperature.

The water vapor flux, separated into isothermal q_{Vh} (pressure head driven) and thermal q_{VT} (temperature driven), is described as:

$$q_V=q_{Vh}+q_{VT}=-D_{Vh}\frac{\partial h}{\partial z}-D_{VT}\frac{\partial T}{\partial z} \quad (3)$$

where D_{Vh} (kg m^{-2} s^{-1}) is the isothermal vapor conductivity; and D_{VT} (kg m^{-1} s^{-1} °C^{-1}) is the thermal vapor diffusion coefficient, presented in Zeng et al. (2011a).

The root water uptake term described by Feddes et al. (1978) is

$$S(h)=\alpha(h)S_p \quad (4)$$

where $\alpha(h)$ (dimensionless) is the reduction coefficient related to soil water potential; and S_p (s^{-1}) is the potential water uptake rate.

$$S_p=b(x)T_p \quad (5)$$

where $b(x)$ is the normalized water uptake distribution, which describes the vertical variation of the potential extraction term, S_p, over the root zone, as described in

Šimůnek et al. (2008).

T_p is the potential transpiration. Following De Vries (1958)'s work, the heat transport function in unsaturated soil can be expressed as

$$\frac{\partial}{\partial t}[(\rho_s\theta_s C_s + \rho_L\theta_L C_L + \rho_V\theta_V C_V)(T-T_r) + \rho_V\theta_V L_0] - \rho_L W\frac{\partial\theta_L}{\partial t} = \frac{\partial}{\partial z}(\lambda_{eff}\frac{\partial T}{\partial z}) - \frac{\partial q_L}{\partial z}C_L(T-T_r) - \frac{\partial q_V}{\partial z}[L_0 + C_V(T-T_r)] - C_L S(T-T_r) \quad (6)$$

where C_s, C_L and C_V (J kg^{-1} °C^{-1}) are the specific heat capacities of solids, liquid and water vapor, respectively; ρ_s (kg m^{-3}) is the density of solids; θ_s is the volumetric fraction of solids in the soil; T_r (°C) is the arbitrary reference temperature; L_0(J kg^{-1}) is the latent heat of vaporization of water at temperature T_r; W (J kg^{-1}) is the differential heat of wetting (the amount of heat released when a small amount of free water is added to the soil matrix); and λ_{eff} (W m^{-1} °C^{-1}) is the effective thermal conductivity of the soil.

Dry air transport in unsaturated soil is originally taken into account in STEMMUS, and the balance equation can be written (Thomas and Sansom, 1995) as

$$\frac{\partial}{\partial t}[\varepsilon\rho_{da}(S_a + H_c S_L)] = \frac{\partial}{\partial t}[D_e\frac{\partial\rho_{da}}{\partial z} + \rho_{da}\frac{S_a K_g}{\mu_a}\frac{\partial P_g}{\partial z} - H_c\rho_{da}\frac{q_L}{\rho_L} + (\theta_a D_{Vg})\frac{\partial\rho_{da}}{\partial z}] \quad (7)$$

where ε is the porosity; ρ_{da} (kg m^{-3}) is the density of dry air; S_a (=1-S_L) is the degree of air saturation in the soil; S_L (=θ_L/ε) is the degree of saturation in the soil; H_c is Henry's constant; D_e (m^2 s^{-1}) is the molecular diffusivity of water vapor in soil; K_g (m^2) is the intrinsic air permeability; μ_a (kg m^{-2} s^{-1}) is the air viscosity; and D_{Vg} (m^2 s^{-1}) is the gas phase longitudinal dispersion coefficient. Note that the effects of dry air movement are not considered in the current study.

2.3.2 Initial and boundary conditions

In general, the soil surface water flow boundary can be characterized as a flux-type boundary controlled by atmospheric forcing, including soil evaporation, precipitation

and irrigation.

$$(q_L + q_V)\big|_{z=0} = E_s - \rho_L(P + I) \quad (8)$$

where E_s (kg m^{-2} s^{-1}) is the actual soil evaporation rate; P and I (m s^{-1}) are precipitation and irrigation rate, respectively.

After intense irrigation or precipitation, ponding would occur at the soil surface, with the surface boundary thus changing into a pressure-type boundary. It was assumed that surface runoff at the study site was negligible and that the maximum height of the surface ponding layer was 5cm in accordance with the lysimeter structure (**Fig.1**). Since there is a filter layer at the bottom of the soil profile (**Fig.1**), saturated water can be easily drained out of the lysimeter. The bottom boundary was considered a seepage face condition (Šimůnek et al., 2008). The soil surface temperature deduced from the in-situ measurements was used as upper boundary condition for heat transfer, and the bottom temperature was used as lower boundary condition. The initial soil moisture and temperature profile could be determined by interpolating the measured values at the starting date.

2.3.3 Transpiration and soil evaporation

(1) Calculation of the ET_{ind} method

Two different parameterizations of ET components are adopted in land surface models. A common procedure is based on reference crop evapotranspiration (ET_0), which is then partitioned into soil evaporation and transpiration using crop factors (Feddes et al., 1974; Šimůnek et al., 2008; Wu et al., 1999), and noted as the ET_{ind} method.

$$ET_0 = \frac{0.408(R_n - G) + \gamma \dfrac{900}{T_a + 273} u_2 (e_s - e_a)}{\Delta + \gamma(1 + 0.34u_2)} \quad (9)$$

where ET_0 (mm day^{-1}) is the reference ET; R_n (MJ m^{-2} day^{-1}) is the net radiation at the crop surface; G (MJ m^{-2} day^{-1}) is the soil heat flux density; T_a (°C) is the air

temperature at 2m height; u_2 (m s^{-1}) is the wind speed at 2m height (which can be obtained from wind speed data at 10m height using a logarithmic wind profile function); e_a and e_s (kPa) are the actual and saturation vapour pressure, respectively; Δ (kPa °C^{-1}) is the slope of the vapor pressure curve; γ (kPa °C^{-1}) is the psychrometric constant.

The potential transpiration (T_p) can be estimated by multiplying ET_0 with the crop basal coefficient K_{cb}, describing the difference between actual and reference crop surface.

$$T_p = K_{cb} ET_0 \tag{10}$$

Several research studies have related K_{cb} to the dynamics of vegetation (Er-Raki et al., 2007; González-Dugo and Mateos, 2008; Sánchez et al., 2012). The general expression defined by Duchemin et al. (2006) is

$$K_{cb} = K_{cb,max}(1 - \exp(-\tau LAI)) \tag{11}$$

where τ is the extinction coefficient, set at 0.6 (Kemp et al., 1997). Although τ may change slightly in response to structural differences in crop development (Allen et al., 1998; Tahiri et al., 2006), it is convenient to consider τ as a constant (Allen et al., 1998; Shuttleworth and Wallace, 1985; Zhou et al., 2006). $K_{cb,max}$ is the basal crop coefficient at effective full ground cover.

Instead of the evaporation coefficient used in FAO dual K_c-ET_0, we adopted a simple evaporation parameterization similar to in other studies (Feddes et al., 1974; Kemp et al., 1997; Wu et al., 1999), in which the potential soil evaporation is given by Ritchie (1972)

$$E_p = \frac{\Delta}{\lambda(\Delta + \gamma)} R_n \exp(-0.39LAI) \tag{12}$$

where λ (MJ kg^{-1}) is the latent heat of vaporization. Actual soil evaporation can be achieved using a simple relationship proposed by Linacre (1973) and verified by Kemp et al. (1997) for bare soil. Three successive stages are arbitrarily divided into:

$$E_s = E_p \qquad (\theta_1 / \theta_{1,Fc}) > (E_p / k)^{1/2}, h_1 > -100000cm$$

$$E_s = k(\theta_1 / \theta_{1,Fc})^m \qquad (\theta_1 / \theta_{1,Fc}) \le (E_p / k)^{1/2}, h_1 > -100000cm \qquad (13)$$

$$E_s = k(\theta_{1+2} / \theta_{1+2,Fc})^m \qquad h_1 \le -100000cm$$

where θ_1 and $\theta_{1,\,Fc}$ are the actual volumetric water content and water content at field capacity of the top soil layer, respectively; h_1 (cm) is the water potential of the top soil layer; k and m are parameters primarily dependent on soil depth and soil texture, varying from 0.8 to 1 and 2 to 2.3, respectively, for a soil depth of 10 to 20cm; θ_{1+2} and $\theta_{1+2,\,Fc}$ are the actual volumetric water content and water content at field capacity of the top 1st and 2nd soil layers, respectively.

(2) Calculation of the ET_{dir} method

The second method used is a one-step calculation of actual soil evaporation and potential transpiration by incorporating canopy minimum surface resistance and actual soil resistance into the Penman-Monteith model. LAI is implicitly used to partition available energy into canopy and soil. We call it the ET_{dir} method. Contrary to an alternative approach proposed by Shuttleworth and Wallace (1985), the interactive effect between canopy and soil was assumed negligible in the ET_{dir} method. This simplification seemed reasonable, as Kemp et al. (1997) indicated that no significant difference in simulating transpiration and soil evaporation was found for both methods.

$$T_p = \frac{\Delta(R_n^c - G) + \rho_a c_p \dfrac{(e_s - e_a)}{r_a^c}}{\lambda(\Delta + \gamma(1 + \dfrac{r_{c\min}}{r_a^c}))} \qquad (14)$$

$$E_s = \frac{\Delta(R_n^s - G) + \rho_a c_p \dfrac{(e_s - e_a)}{r_a^s}}{\lambda(\Delta + \gamma(1 + \dfrac{r_s}{r_a^s}))} \qquad (15)$$

where R_n^c and R_n^s (MJ m^{-2} day^{-1}) are the net radiation at the canopy surface and soil surface, respectively; ρ_a (kg m^{-3}) is the air density; c_p (J kg^{-1} K^{-1}) is the specific heat capacity of air; r_a^c and r_a^s (s m^{-1}) are the aerodynamic resistance for canopy surface and bared soil, respectively; r_{cmin} (s m^{-1}) is the minimum canopy surface resistance; and r_s (s m^{-1}) is the soil surface resistance.

The net radiation reaching the soil surface can be calculated using the Beer's law:

$$R_n^s = R_n \exp(-\tau LAI) \tag{16}$$

And the net radiation intercepted by the canopy surface is the residual part of total net radiation

$$R_n^c = R_n (1 - \exp(-\tau LAI)) \tag{17}$$

The minimum canopy surface resistance r_{cmin} is given by

$$r_{c\min} = r_{l\min} / LAI_{eff} \tag{18}$$

where r_{lmin} is the minimum leaf stomatal resistance; LAI_{eff} is the effective leaf area index, which considers that generally the upper and sunlit leaves in the canopy actively contribute to the heat and vapor transfer.

The soil surface resistance can be estimated using an exponential form proposed by Van De Griend and Owe (1994),

$$\begin{aligned} r_s &= r_{sl} && \theta_1 > \theta_{\min}, h_1 > -100000cm, \\ r_s &= r_{sl} e^{a(\theta_{\min} - \theta_1)} && \theta_1 \le \theta_{\min}, h_1 > -100000cm \\ r_s &= \infty && h_1 \le -100000cm \end{aligned} \tag{19}$$

where r_{sl} (10 s m^{-1}) is the resistance to molecular diffusion of the water surface; a (0.3565) is the fitted parameter; θ_1 is the topsoil water content; $\theta_{min}$is the minimum water content above which soil is able to deliver vapor at a potential rate.

2.4 Model Parameters

2.4.1 Soil property parameters

Van Genuchten's analytical model (Van Genuchten, 1980) was used to simulate the soil moisture retention curve, which describes the relationship between soil water potential and water content. Soil samples of the top 20cm were taken to obtain the parameters for the moisture retention curve.

Soil saturated hydraulic conductivity could be determined at the laboratory, and was 10.50 cm d^{-1}. This value is lower than the value recommended by Saxton et al. (1986) value for silt clay loam (13.60 cm d^{-1}), but is within the range of 10.30 to 14.30 cm d^{-1}, given by Wang et al. (2008) for the local soil. The soil hydraulic and thermal properties are presented in **Table 2**.

2.4.2 Crop growth parameters

LAI was determined using the measured leaf area. To simulate the seasonal dynamics in LAI, a linear interpretation was used between dates from the emergence to the first measurement and a simple quadratic function presented a good fit for the LAI measurements (R^2=0.96) (**Fig. 2a**). The effective leaf area index (LAI_{eff}), used in the ET_{dir} method, was equal to the actual LAI where the LAI was lower than 2 m^2 m^{-2}, was assumed to be half the actual LAI for actual LAI values above 4 m^2 m^{-2} and equal to 2 m^2 m^{-2} where actual LAI values ranged between 2 to 4 m^2 m^{-2} (Tahiri et al., 2006).

Maximum rooting depth was set to 1.2m, in accordance with Allen et al. (1998). A classical logistic growth function was used to estimate root growth dynamics throughout the growing season, in which the root growth rate was determined from the assumption that 50% of the rooting depth would be reached after 50% of the growing season had elapsed, as described in Šimůnek et al. (2008) (see **Fig. 2c** for the root growth dynamics). The normalized water uptake distribution *b(x)*, which describes the vertical variation of the potential extraction term, S_p, over the root zone

was determined following Šimůnek et al. (2008).

A piecewise linear function, defined in Feddes et al.(1978) and Feddes and Roats (2004), was used to describe the response of root to soil water potential $\alpha(h)$. The input water potential parameters were: i) -15 cm for the water potential below which roots start to extract water; ii) -30 cm for the water potential below which roots extract water at the maximum possible rate; iii) higher limit -325 cm and lower limit -600 cm for the limiting water potential values below which roots can no longer extract water at the maximum rate (assuming a potential transpiration rate of 0.5 and 0.1 cm d^{-1}, respectively); iv) -15000 cm for the water potential below which root water uptake ceases.

2.5 Numerical Simulations and Experiments

The extended STEMMUS model was run using both the ET_{ind} method and the ET_{dir} method. Coupled water flow and heat transport equations were numerically solved using the Galerkin's finite element method for the spatial discretization and using a fully implicit, backward difference approach for the temporal discretization. Plant root water uptake and soil water flow were fully coupled and equations were solved simultaneously at the same time step. The soil profile considered in this study had a depth of 3m, equal to that of the large lysimeter, and was divided into 38 nodes with a finer discretization in the upper soil layers (1cm) than in the lower soil layers (20cm). The large lysimeter measurements, including soil moisture, soil temperature, ET and soil evaporation were used to assess model performance. The validation of the soil water balance closure within the root zone gave an additional test of the effectiveness of the extended STEMMUS. In addition, since the estimation of crop growth parameters could harbor uncertainties, a sensitivity test was implemented to explore how the simulation results varied with fluctuating precipitation and irrigation under different crop growth scenarios.

2.5.1 Water balance closure

The water balance closure was implemented by comparing soil water storage using two different methods. The direct method was based on the summation of soil water content over the root-zone

$$V_t = \sum_{rz} \Delta x_i \frac{\theta_i + \theta_{i+1}}{2} \tag{20}$$

where V_t is the soil water storage in the root zone at time t; Δx_i is the thickness of the ith soil layer; θ_i and θ_{i+1} are model simulations of water content at the upper and lower surface, respectively, of the ith soil layer, at time t; $\sum_{rz}$ represents the summation over the root zone.

Soil water storage could also be derived by the inversion of the water balance equation within the root-zone

$$V_t = V_0 - \int_0^t T_c dt + \int_0^t (q_0 - q_N) dt \tag{21}$$

where V_0 is the soil water storage in the root zone at the initial time, calculated by the integration of the initial soil moisture over the root zone; T_c is the actual crop transpiration, derived from the integration of root water uptake over the root zone; q_0 and q_N are the simulated water fluxes at the surface and base of the root zone, respectively.

2.5.2 Crop growth scenarios

To investigate how biological factors control shallow soil water dynamics, three additional crop growth scenarios were used: i) a changed leaf area index, ii) a changed maximum rooting depth (Z_{rmax}), and iii) a changed root growth rate (R_{gr}) scenario. The reference scenario (REF) was compared with these changed LAI ($LAI/LAI_{\_ref}$), Z_{rmax}, and R_{gr} (Z_r/ Z_{r_ref}) scenarios to demonstrate the impact changes in biological factors may have. To select values for these three growth parameters their reference values were either increased or decreased by 20%. The influence of such a 20% increase and

363 decrease in LAI, Z_{rmax}, and R_{gr} is shown in **Fig. 2**. The influence of a 20% increase in
364 the LAI on the relative LAI_{eff} encompassed three stages: i) a constant 1.2 times
365 enlarged stage, ii) a constantly equal stage, and iii) a transition stage (**Fig. 2b**). The
366 influence of a 20% decrease in the LAI depicted a similar three-stage trend. However,
367 the 20% decreased LAI scenario (**Fig. 2b**, dash grey line) entered stage (ii), i.e. the
368 constantly equal stage, later in the leaf growing stage and earlier in the leaf senescing
369 stage, than the 20% increased LAI scenario (**Fig. 2b**, solid grey line) did. Compared
370 to the reference root depth dynamics, the relative values of root depth (Z_r/ Z_{r_ref}) of the
371 20% increased Z_{rmax} scenario, increased gradually until it reached its maximum value
372 late in the growing season. In the 20% increased R_{gr} scenario, the Z_r/ Z_{r_ref}
373 demonstrated a rapid increase up to a maximum value and then dropped down during
374 the late growing season. On the other hand, a 20% decrease in Z_{rmax} and R_{gr} showed
375 opposite trends to the 20% increase on the relative root depth dynamics. A 20%
376 decreased R_{gr} showed a lag effect for the Z_r/ Z_{r_ref}, compared to the 20% increased R_{gr}
377 (**Fig. 2d**). In other words, the values of Z_r/ Z_{r_ref} for the 20% decreased R_{gr} scenario
378 were lower early in the growing season (before around DOY 196) and higher late in
379 the growing season (after around DOY 196) than for the 20% increased R_{gr} scenario.

380 ## 2.6 Performance Matrixes

381 To assess the model performance, several performance matrixes were used similar to
382 in previous studies (Wei et al., 2015; Zhao et al., 2013). The determination coefficient
383 R^2, achieved by performing a linear regression between observed and model simulated
384 values; the root mean square error (RMSE), characterizing the variance of the model
385 errors; as well as the index of agreement (d-index) (Willmott, 1981; Willmott et al.,
386 1985) have been computed as follows:

$$RMSE = \sqrt{\frac{\sum_{i=1}^{n}\left(P_i - O_i\right)^2}{n}} \tag{22}$$

$$R^2 = \frac{\left[\sum_{i=1}^{n}\left(P_i - \overline{P}\right)\left(O_i - \overline{O}\right)\right]^2}{\sum_{i=1}^{n}\left(P_i - \overline{P}\right)^2 \sum_{i=1}^{n}\left(O_i - \overline{O}\right)^2} \quad (23)$$

$$d = 1 - \frac{\sum_{i=1}^{n}\left(P_i - O_i\right)^2}{\sum_{i=1}^{n}\left(\left|P_i - \overline{O}\right| + \left|O_i - \overline{O}\right|\right)^2} \quad (24)$$

where n is the number of observations, P_i and O_i are pairs of observed and model predicted values for a specific variable (soil water content, ET, etc.), $\overline{P}$ and $\overline{O}$ are the overall mean of observed and model predicted values. Good agreement between observed and model predicted values is characterized by a high value for both the determination coefficient and the d-index, and a low value for the RMSE.

3 Results and discussion

3.1 Soil water content

Simulated soil water content, based on two ET methods, was compared with observations at soil depths of 20cm, 40cm, 60cm, 80cm and 100cm (**Fig. 3**). The soil water content at 20cm derived from the ET_{ind} method was in good agreement with the observation. Though slight underestimation occurred in the initial stage, the effects of incoming water flux (precipitation and irrigation) on soil water dynamics were well represented, as evidenced by a d-index of 0.81 and RMSE of 0.017 $cm^3\ cm^{-3}$. For the deeper soil layers, however, the sensor-observed fluctuations in soil water content were much smaller than the simulated values, thus inducing large discrepancies. The d-index values ranged from 0.26 to 0.66 and the RMSE ranged from 0.019 to 0.025 $cm^3\ cm^{-3}$ for soil depths of 40cm to 100cm.

The results for soil water content simulated employing the ET_{dir} method were similar to those based on the ET_{ind} method (**Fig. 3**). However, owning to more underestimation, the model based on the ET_{dir} method performed a little worse than

407 the model based on the ET_{ind} method. The d-index values ranged from 0.20 to 0.73
408 and the RMSE ranged from 0.020 to 0.036 cm^3 cm^{-3} for the soil depths of 20cm to
409 100cm.

410 For both ET methods, the extended STEMMUS model underestimated soil water
411 content early in the growing season. From the point of water balance, this
412 underestimation may be explained by more soil water consumption mainly due to
413 topsoil evaporation, indicating that both ET methods overestimated soil evaporation
414 early in the growing season. The other possible reason was that too little irrigation
415 was applied during this period to obtain uniform distribution, resulting in single-point
416 soil moisture observation losing its ability to represent the heterogeneous soil
417 moisture variations. Such underestimation disappeared when a large amount of water
418 was applied late in the growing season (**Fig. 3, 20cm**).

419 The discrepancies increased with soil depth for both ET methods. The reason may be
420 twofold. On the one hand, the soil moisture observations were doubtful, as, with
421 irrigation, no significant fluctuation occurred at the deeper soil layers, which was also
422 inconsistent with other results for the same experimental site (Kang et al., 2001). The
423 unreliable observations may be linked to the positioning of the soil moisture sensors
424 (either installed at positions dominated by preferential flow or adjacent to
425 macropores). On the other hand, the assumption of a homogeneous soil texture was
426 inappropriate, as was discussed in previous studies (Zeng et al., 2011a). Soil hydraulic
427 parameters controlled the liquid water flux partitioning through the soil layers. A
428 larger infiltration rate could result in greater fluctuation in soil water content at deeper
429 soil layers.

430 ### 3.2 Root zone water balance

431 Applying equations (20) and (21), simulated soil water storage based on the
432 integration of soil water content and the inversion of the water balance equation over
433 the root-zone, using two ET methods, are compared in **Fig. 4**. Soil water storage
434 calculated both ways agreed well for the ET_{ind} method. The value of the RMSE was

435 5.88 mm and the d-index value was 0.98. Similarly, good agreement was found using
436 the ET_{dir} method with values for the RMSE and the d-index equaling 5.13mm and
437 0.99, respectively. Overall, the results based on the performance matrixes and the
438 visual comparison of soil water storage dynamics revealed that the numerical solution
439 using both the ET_{ind} and ET_{dir} method effectively reproduced the closure of the water
440 balance even under dramatically changed surface boundary flux conditions.

441 Simulated results using two ET methods showed similar trends in soil water storage
442 throughout the growing season (**Fig. 4**). As expected, the greatest increases occurred
443 after large irrigations. Using the ET_{dir} method tended to result in lower soil water
444 storage than using the ET_{ind} method. Differences between the two ET methods
445 generally increased with drying of the soil.

446 ### 3.3 Soil temperature

447 **Figure 5** presents the dynamics of sensor-observed and the simulated soil temperature
448 using two ET methods at various soil depths. Compared to the observation, the
449 simulation started with good agreement for both ET methods, followed by a slight
450 overestimation after the first main irrigation. Irrigation events had a significant impact
451 on the soil temperature simulation due to the uncertainties in soil surface temperature.
452 Nevertheless, the seasonal variations in soil temperature could be satisfactorily
453 portrayed with both ET methods. The overall d-index values, for soil depths of 20cm
454 to 100cm, ranged from 0.76 to 0.95 using the ET_{ind} method and from 0.78 to 0.95
455 using the ET_{dir} method. The RMSE values ranged from 1.19 to 1.71 ℃ using the ET_{ind}
456 method and from 1.14 to 1.61 ℃ using the ET_{dir} method for these same soil depths of
457 20cm to 100cm.

458 ### 3.4 Estimation of ET

459 Combined with simulation results for soil water content, accurate ET estimates could
460 help with the visualization of soil water balance, reduce deep percolation, improve
461 irrigation efficiency and ultimately optimize water resources management. Therefore,

462 the capability of the extended STEMMUS model with different ET methods in
463 reproducing the dynamics of ET is of great importance and requires a thorough
464 evaluation with observed ET data.

465 3.4.1 ET at hourly time scale

466 The performance of both ET methods in estimating the diurnal pattern of ET
467 throughout the growing season is shown in **Fig. 6** and **Table 3**. Hourly ET rates
468 simulated using the ET_{dir} method generally agreed well with lysimeter-observed ones
469 (**Fig. 6**). There was no significant underestimation throughout the growing season.
470 The results summarized in **Table 3** suggest that the main disagreement for the ET_{dir}
471 method occurred during the early growing stage. The values for the d-index were 0.90,
472 0.96, 0.98 and 0.93 and for the RMSE were 0.10 mm h^{-1}, 0.09 mm h^{-1}, 0.08 mm h^{-1},
473 and 0.06 mm h^{-1} for the initial, the crop development, the mid-season and the late
474 season growing stages, respectively.

475 Compared to the ET_{dir} method, no significant difference occurred for the ET_{ind} method
476 when the values of ET rates were small (**Fig. 6**). However, more underestimation was
477 found when simulating higher ET values. The greatest disagreement occurred during
478 the initial growing stage with the values of the d-index and the RMSE being 0.84 and
479 0.10 mm h^{-1}, respectively, compared to 0.94 and 0.11 mm h^{-1}, 0.93 and 0.11 mm h^{-1},
480 and 0.90 and 0.07 mm h^{-1}, respectively, during other developmental stages.

481 3.4.2 ET at daily time scale

482 Compared to lysimeter observed daily ET rates, both ET methods showed similar
483 trends over the entire growing season (**Fig. 7**). When neglecting the effects of clouds
484 on the net radiation, large overestimation of ET rates for both schemes occurred on
485 some cloudy days (**Fig. 7**, DOY 196, 197, 221 and 241). Daily ET rates showed more
486 variability when simulated with the ET_{dir} method than with the ET_{ind} method.
487 Moreover, the crop stage-specific behavior differed between the two ET methods.
488 There was an average underestimation with the ET_{ind} method, while a slight
489 overestimation with the ET_{dir} method, during the initial crop development stage. Daily

ET rates during the mid-season stage tended to be underestimated by the ET_{ind} method, while successfully described by the ET_{dir} method. Overall, with daily simulated ET rates the ET_{dir} method performed better than the ET_{ind} method, as is indicated by the d-index and RMSE values of 0.96 and 0.74 mm d^{-1}, respectively, for the ET_{dir} method, compared to 0.89 and 1.06 mm d^{-1}, respectively, for the ET_{ind} method.

Observed soil evaporation by the micro-lysimeter was used to assess the performance of both ET methods in simulating soil evaporation (**Fig. 8**). Statistical results indicated the ET_{dir} method was in closer agreement with the observations than the ET_{ind} method, with RMSE and d-index values for the ET_{dir} method being 0.51mm d^{-1} and 0.84, respectively, compared to 0.73mm d^{-1} and 0.64, respectively, for the ET_{ind} method. Unfortunately, during the period between two supplemental irrigations in the early growing season (DOY 177-183), no soil evaporation measurements by the micro-lysimeter were available. Thus, it was difficult to form a conclusion regarding model performance during this period. Late in the growing season, both ET methods tended to underestimate daily evaporation rates after main irrigation events. This underestimation may be caused by the use of the micro-lysimeter. The observed soil evaporation may have been higher than the actual soil evaporation, since the micro-lysimeter disregarded the soil water loss due to the root water extraction in the evaporative soil layer. Similar behavior was reported for maize by Zhao et al. (2013) and Wei et al. (2015) at same latitude sites. Compared to the ET_{dir} method, using the ET_{ind} method resulted in much lower values for the rate of evaporation, especially after irrigation during the initial and mid-late crop development stage (see also **Table 4**). During these periods, the local irrigation intensified the vertical vapor gradient and the relative sparse vegetation cover highlighted the importance of the aerodynamics component. Thus, larger underestimation and less fluctuation of soil evaporation using the ET_{ind} method could be partially explained by the simplification of aerodynamic and surface resistance components in the calculation.

3.4.3 Cumulative ET

A comparison between cumulative observed ET and simulated ET, using both the

519 ET_{ind} and the ET_{dir} method, is shown in **Fig. 9**. The cumulative ET observed by the
520 lysimeter, as well as simulated using the ET_{ind} and the ET_{dir} methods, were 334.18,
521 354.89 and 369.37mm, respectively. Both ET methods overestimated seasonal ET
522 compared to the lysimeter observations. Two periods, i.e. crop development and late
523 season stage, contributed to the overestimation by the ET_{ind} method. While, for the
524 ET_{dir} method, the initial and crop development stage accounted for 70% of the
525 overestimation (**Table 4**). The deviation from the observed value of total ET was
526 greater for the ET_{dir} method than for the ET_{ind} method, i.e. 35.18mm and 20.71mm,
527 respectively. This nearly 15mm difference is mainly attributed to the larger amount of
528 evaporation determined by the ET_{dir} method during the initial growth stage (**Table 4**),
529 consequently resulting in more severe soil water depletion (**Fig. 3, 20cm**).

530 ### 3.4.4 Characteristics of ET partitioning

531 Crop stage-specific soil evaporation (E), plant transpiration (T_c), evapotranspiration
532 (ET) and evaporation fraction (E/ET, EF) are presented in **Table 4**. Similar to
533 previous studies (Kang et al., 2003; Zhao et al., 2013), the proportion of evaporation
534 (the evaporation fraction) was largest at the initial stage, then decreased during crop
535 development and reached its lowest value at the mid-season stage, with a significant
536 rebound occurring during the late season. The dynamic role of evaporation was
537 mainly attributed to crop vegetation development (Hu et al., 2009; Liu et al., 2002).
538 The evaporation fraction of the four development stages ranged between 24.38% and
539 86.58% for the ET_{dir} method and between 10.31% and 81.01% for the ET_{ind} method,
540 similar to previously published results (Paredes et al., 2015; Wei et al., 2015; Zhao et
541 al., 2013). Some differences were found in simulating individual components of crop
542 ET when using the two different ET methods. The ET_{dir} method showed a greater
543 evaporation and less transpiration than the ET_{ind} method throughout the growing
544 season, resulting in an overall larger evaporation fraction.

545 The overall evaporation fractions for the two ET methods used were 24.05% (ET_{ind})
546 and 36.44% (ET_{dir}). Figures that are below the range of 43.57% to 52.52% of a 4-year
547 field observation study in the same region that saw a significantly higher frequency of

548 wetting events (Wang et al., 2007), but close to observations by Liu et al. (2002) of
549 30.3% and Kang et al. (2003) of 33%, and within the range of 20 % to 40 %, reviewed
550 by Kool et al. (2014) for most of row crops.

551 ### 3.5 Crop growth scenarios

552 To investigate the uncertainty in crop growth parameters, different crop growth
553 scenarios, introduced in section 2.5.2, were adopted to run the STEMMUS with both
554 ET methods (**Fig. 10**). The reference scenario (REF) was compared to the changed
555 LAI, Z_{rmax}, and R_{gr} scenarios. The relative values (i.e. $T_c/T_{c,ref}$ & EF/EF_{ref}) were used
556 here to facilitate comparisons between parameters and scenarios.

557 Under the changed LAI scenario, the dynamics of seasonal relative values of
558 transpiration ($T_c/T_{c,ref}$) formed a tradeoff between increasing LAI and decreasing soil
559 water availability, while other factors remained unchanged throughout the growing
560 season. **Fig. 10a** shows that, for the ET_{ind} method, the sensitivity of transpiration to
561 LAI decreased until its value approached 2 m^2 m^{-2}, then leveled off with both factors
562 being of equal importance and finally elevated as soil water availability was
563 decreasing. For the ET_{ind} method, the influence of LAI was more important in the
564 early growing season, which is consistent with previous studies. In **Fig. 10g**, the
565 dynamics of the relative evaporation fraction (EF/EF_{ref}) show a trend similar to the
566 seasonal variation of the LAI (**Fig. 2a**), indicating that small differences in soil water
567 availability appeared to have a negligible effect on the relative evaporation fraction
568 (EF/EF_{ref}) over the entire growing season. The LAI dynamics could explain much of
569 the seasonal variation in the relative EF. It is worth to note that there was an
570 asymmetric variation in the relative EF for the same LAI disturbance, indicating that
571 the EF was nonlinearly dependent on LAI disturbance **(Fig. 10g)**.

572 With the ET_{dir} method, the relative transpiration presented more complicated behavior
573 than with the ET_{ind} method **(Fig. 10d)**. Compared to the ET_{ind} method, the ET_{dir}
574 method revealed a similar trend in the sensitivity of relative transpiration to LAI in the
575 early growing season, when LAI dominated. More fluctuation was visible in the

middle season. A suppression effect appeared at the end of the growing season (i.e. increasing LAI resulted in lower transpiration). This behavior could be explained by the selection of a different LAI in estimating transpiration for the two ET methods, i.e LAI for the ET_{ind} method, and LAI_{eff} for the ET_{dir} method (**Fig. 2a**). The response of relative EF to LAI showed similar trends early in the growing season between the ET_{ind} method and the ET_{dir} method, though with less sensitivity in the ET_{dir} method. Differences were found late in the growing season with a negligible effect of LAI on the relative EF in the senescing maize **(Fig. 10j)**.

Under the changed maximum rooting depth and root growth rate scenarios, the interactive effects of root depth dynamics and soil water availability on transpiration and the evaporation fraction were explored. Seasonal transpiration ratio was an increasing function of soil water depletion until reaching a threshold in both scenarios. The effects of changed maximum rooting depth on relative transpiration and the evaporation fraction increased, as the soil was drying. Larger sensitivity was found late in the growing stage. On the contrary, the influence of the soil drying on the sensitivity of transpiration and the evaporation fraction to root growth rate decreased until no significant effects were found when the root reached its maximum depth. The period most influenced occurred early in the growing season. This behavior can be explained by the difference in root depth dynamics in both scenarios. As shown in **Fig. 2c** and **d**, the effect of maximum rooting depth increased until reach its maximum value late in the growing season, while the effect of root growth rate primarily dominated early in the growing season. Furthermore, there was an asymmetric variation in the relative transpiration and evaporation fraction for equal disturbance of root growth rate, with a larger variation for conditions of 20% decreased root growth rate and less variation for the increased conditions (especially at DOY 225, in **Fig. 10c, f, i, l**). Such asymmetric variation can be explained by the lag effect described in section 2.5.2. The two ET methods differed in their variation in sensitivity to root growth parameters, with higher sensitivity observed in the ET_{dir} method with equal parameter disturbance. This is probably due to the fact that the ET_{dir} method is more

sensitive to soil water depletion than the ET_{ind} method (**Fig. 3**), considering aerodynamic and surface resistance.

Based on the crop growth scenario results, some suggestions may be presented to reduce the proportion of soil evaporation in the total evapotranspiration. Under the same irrigation and atmospheric forcing conditions, the leaf area index can be increased by properly increasing the planting density (**Fig. 10g, j**). Unlike the LAI, the sensitivity of transpiration to root growth parameters depended more on soil water depletion, which indicated that the effects of dynamic root growth parameters should not be dismissed in an arid environment. In fact, a variety of maximum rooting depth values were reported for maize previously (Canadell et al., 1996; Hsiao et al., 2009; Liu et al., 1998), due to differences in genotypes and rhizosphere environment. Under conditions of soil drying, plants tend to increase root depth to maintain a certain amount of water extraction (Hund et al., 2009; Verma et al., 2014), as evidenced in **Fig. 10b-c & e-f**.

4 Summary and Conclusion

Together with the in situ data collected in a large lysimeter experiment in a semi-arid environment, the extended STEMMUS model facilitated the investigation of how the coupling transfer of water, vapor and heat in the soil affected soil water dynamics in a crop field, using two different evapotranspiration methods (ET_{ind} & ET_{dir}). The simulated soil water content values based on the ET_{ind} method were in closer agreement with values measured at 20cm soil depth than values based on the ET_{dir} method. However, disagreement increased in deeper soil layers, with either the inaccuracy of soil moisture observations or the heterogeneity of soil hydraulic parameters being responsible for the discrepancies and requiring further investigation. The simulation of soil temperature performed relatively well for both ET methods.

Evaluation of the performance of the two ET methods in estimating hourly, daily and cumulative evapotranspiration demonstrated that the ET_{dir} method performed better than the ET_{ind} method, except regarding the cumulative evapotranspiration, with the ET_{dir} method displaying a 15mm higher overestimation than the ET_{ind} method,

compared to the lysimeter observations. Caution should be exercised in partitioning ET, because individual ET components (soil evaporation, transpiration) were not fully or accurately measured. This study suggests that the ET_{dir} method provides a better simulation of soil evaporation than the ET_{ind} method, especially late in the growing season. It confirms that aerodynamic and surface resistance terms are necessary for evaporation estimation.

The crop growth scenario results revealed the interactive effects of LAI, maximum rooting depth and root growth rate with soil water availability on relative transpiration and the evaporation fraction. When it was less than 2 m^2 m^{-2}, the LAI played an important role in controlling transpiration. The effects of maximum rooting depth and root growth rate only appeared in drying periods, with the first being more important late in the growing season, while the latter dominated early in the growing season. As the disturbance of crop growth parameters has a significant effect on the simulation results, further consideration of the dynamics of crop growth parameters in a changing environment is needed.

Acknowledgements. This research was supported by the National Natural Science Foundation of China (Grant No. 51179162) and the 111 Project of Chinese Education Ministry (No. B12007). We thank the anonymous referees very much for improving the manuscript. L. Yu is grateful for the financial support by the China Scholarship Council (CSC), No. 201406300115.

References

Allen, R. G., Pereira, L. S., Raes, D., and Smith, M.: Crop evapotranspiration-Guidelines for computing crop water requirements-FAO Irrigation and drainage paper 56, FAO, Rome, 300pp, 1998.

Anothai, J., Soler, C. M. T., Green, A., Trout, T. J., and Hoogenboom, G.: Evaluation of two evapotranspiration approaches simulated with the CSM-CERES-Maize model under different irrigation strategies and the impact on maize growth, development and soil moisture content for semi-arid conditions, Agr. Forest Meteorol., 176, 64-76, 2013.

Bittelli, M., Ventura, F., Campbell, G. S., Snyder, R. L., Gallegati, F., and Pisa, P. R.: Coupling of heat, water vapor, and liquid water fluxes to compute evaporation in bare soils, J. Hydrol., 362, 191-205, 2008.

Boast, C. W., and Robertson, T. M.: A "Micro-Lysimeter" Method for Determining Evaporation from Bare Soil: Description and Laboratory Evaluation, Soil Sci. Soc. of Am. J., 46, 689-696, 1982.

Canadell, J., Jackson, R. B., Ehleringer, J. B., Mooney, H. A., Sala, O. E., and Schulze, E. D.: Maximum rooting depth of vegetation types at the global scale, Oecologia, 108, 583-595, 1996.

Chen, J., Chen, B., Black, T. A., Innes, J. L., Wang, G., Kiely, G., Hirano, T., and Wohlfahrt, G.: Comparison of terrestrial evapotranspiration estimates using the mass transfer and Penman-Monteith equations in land surface models, J. Geophys. Res.-Biogeo., 118, 1715-1731, 2013.

De Vries, D. A.: Simultaneous transfer of heat and moisture in porous media, EOS T. Am. Geophys. Un., 39, 909-916, 1958.

De Vries, D. A.: Thermal properties of soils, Physics of Plant Environment, edited by: van Wijk, W. R., North-Holland Publishing Company, Amsterdam, 1963.

Duchemin, B., Hadria, R., Erraki, S., Boulet, G., Maisongrande, P., Chehbouni, A.,

684 Escadafal, R., Ezzahar, J., Hoedjes, J. C. B., Kharrou, M. H., Khabba, S., Mougenot,
685 B., Olioso, A., Rodriguez, J. C., and Simonneaux, V.: Monitoring wheat phenology
686 and irrigation in Central Morocco: On the use of relationships between
687 evapotranspiration, crops coefficients, leaf area index and remotely-sensed
688 vegetation indices, Agr. Water Manage., 79, 1-27, 2006.

689 Er-Raki, S., Chehbouni, A., Guemouria, N., Duchemin, B., Ezzahar, J., and Hadria, R.:
690 Combining FAO-56 model and ground-based remote sensing to estimate water
691 consumptions of wheat crops in a semi-arid region, Agr. Water Manage., 87, 41-54,
692 2007.

693 Ershadi, A., McCabe, M. F., Evans, J. P., and Wood, E. F.: Impact of model structure
694 and parameterization on Penman-Monteith type evaporation models, J. Hydrol.,
695 525, 521-535, 2015.

696 Feddes, R. A., Bresler, E., and Neuman, S. P.: Field test of a modified numerical
697 model for water uptake by root systems, Water Resour. Res., 10, 1199-1206, 1974.

698 Feddes, R. A., Kowalik, P. J., and Zaradny, H.: Simulation of field water use and crop
699 yield, Centre for Agricultural Publishing and Documentation, Wageningen, the
700 Netherlands, 1978.

701 Feddes, R. A., and Roats, P. A. C.: Parameterizing the soil-water-plant root system, in:
702 Unsaturated-Zone Modeling: Progress, Challenges and Applications, edited by:
703 Feddes, R. A., DeRooij, G. H., and VanDam, J. C., Kluwer Academic Publishers,
704 Dordrecht, the Netherlands, 95-141, 2004.

705 Federer, C. A., Vörösmarty, C., and Fekete, B.: Intercomparison of methods for
706 calculating potential evaporation in regional and global water balance models,
707 Water Resour. Res., 32, 2315-2321, 1996.

708 Federer, C. A., Vörösmarty, C., and Fekete, B.: Sensitivity of annual evaporation to
709 soil and root properties in two models of contrasting complexity, J. Hydrometeorol.,
710 4, 1276-1290, 2003.

González-Dugo, M. P., and Mateos, L.: Spectral vegetation indices for benchmarking water productivity of irrigated cotton and sugarbeet crops, Agr. Water Manage., 95, 48-58, 2008.

Hsiao, T. C., Heng, L., Steduto, P., Rojas-Lara, B., Raes, D., and Fereres, E.: AquaCrop—The FAO crop model to simulate yield response to water: III. Parameterization and testing for maize, Agron. J., 101, 448-459, 2009.

Hu, Z., Yu, G., Zhou, Y., Sun, X., Li, Y., Shi, P., Wang, Y., Song, X., Zheng, Z., Zhang, L., and Li, S.: Partitioning of evapotranspiration and its controls in four grassland ecosystems: Application of a two-source model, Agr. Forest Meteorol., 149, 1410-1420, 2009.

Hund, A., Ruta, N., and Liedgens, M.: Rooting depth and water use efficiency of tropical maize inbred lines, differing in drought tolerance, Plant Soil, 318, 311-325, 2009.

Kang, S., Zhang, F., and Zhang, J.: A simulation model of water dynamics in winter wheat field and its application in a semiarid region, Agr. Water Manage., 49, 115-129, 2001.

Kang, S., Gu, B., Du, T., and Zhang, J.: Crop coefficient and ratio of transpiration to evapotranspiration of winter wheat and maize in a semi-humid region, Agr. Water Manage., 59, 239-254, 2003.

Kemp, P. R., Reynolds, J. F., Pachepsky, Y., and Chen, J. L.: A comparative modeling study of soil water dynamics in a desert ecosystem, Water Resour. Res., 33, 73-90, 1997.

Kool, D., Agam, N., Lazarovitch, N., Heitman, J. L., Sauer, T. J., and Ben-Gal, A.: A review of approaches for evapotranspiration partitioning, Agr. Forest Meteorol., 184, 56-70, 2014.

Linacre, E. T.: A simpler empirical expression for actual evapotranspiration rates — a discussion, Agr. Meteorol., 11, 451-452, 1973.

738 Liu, C., Zhang, X., and Zhang, Y.: Determination of daily evaporation and
739 evapotranspiration of winter wheat and maize by large-scale weighing lysimeter
740 and micro-lysimeter, Agr. Forest Meteorol., 111, 109-120, 2002.

741 Liu, Y., Teixeira, J. L., Zhang, H. J., and Pereira, L. S.: Model validation and crop
742 coefficients for irrigation scheduling in the North China plain, Agr. Water Manage.,
743 36, 233-246, 1998.

744 Mastrocicco, M., Colombani, N., Salemi, E., and Castaldelli, G.: Numerical
745 assessment of effective evapotranspiration from maize plots to estimate
746 groundwater recharge in lowlands, Agr. Water Manage., 97, 1389-1398, 2010.

747 Milly, P. C. D.: Moisture and heat transport in hysteretic, inhomogeneous porous
748 media: a matric head-based formulation and a numerical model, Water Resour. Res.,
749 18, 489-498, 1982.

750 Padilla, F. L. M., González-Dugo, M. P., Gavilán, P., and Domínguez, J.: Integration
751 of vegetation indices into a water balance model to estimate evapotranspiration of
752 wheat and corn, Hydrol. Earth Syst. Sci., 15, 1213-1225,
753 doil:10.5194/hess-15-1213-2011, 2011.

754 Paredes, P., Wei, Z., Liu, Y., Xu, D., Xin, Y., Zhang, B., and Pereira, L. S.:
755 Performance assessment of the FAO AquaCrop model for soil water, soil
756 evaporation, biomass and yield of soybeans in north china plain, Agr. Water
757 Manage., 152, 57-71, 2015.

758 Richards, L. A.: Capillary conduction of liquids in porous mediums, Physics, 1,
759 318-333, 1931.

760 Ritchie, J. T.: Model for predicting evaporation from a row crop with incomplete
761 cover, Water Resour. Res., 8, 1204-1213, 1972.

762 Saito, H., Šimůnek, J., and Mohanty, B. P.: Numerical analysis of coupled water,
763 vapor, and heat transport in the vadose zone, Vadose Zone J., 5, 784-800, 2006.

764 Sánchez, N., Martínez-Fernández, J., González-Piqueras, J., González-Dugo, M. P.,

765 Baroncini-Turrichia, G., Torres, E., Calera, A., and Pérez-Gutiérrez, C.: Water
766 balance at plot scale for soil moisture estimation using vegetation parameters, Agr.
767 Forest Meteorol., 166-167, 1-9, 2012.

768 Saxton, K. E., Rawls, W. J., Romberger, J. S., and Papendick, R. I.: Estimating
769 Generalized Soil-water Characteristics from Texture, Soil Sci. Soc. of Am. J., 50,
770 1031-1036, 1986.

771 Shuttleworth, W. J., and Wallace, J. S.: Evaporation from sparse crops - an energy
772 combination theory, Q. J. Roy. Meteorol. Soc., 111, 839-855, 1985.

773 Shuttleworth, W. J., and Wallace, J. S.: Calculating the water requirements of
774 irrigated crops in Australia using the matt-shuttleworth approach, T. ASABE, 52,
775 1895-1906, 2009.

776 Šimůnek, J., Šejna, M., Saito, H., Sakai, M., and van Genuchten, M. T.: The
777 HYDRUS-1D software package for simulating the movement of water, heat, and
778 multiple solutes in variably saturated media, version 4.0, HYDRUS software series
779 3, Department of Environmental Sciences, University of California Riverside,
780 Riverside, California, USA, 315pp., 2008.

781 Stannard, D. I.: Comparison of Penman-Monteith, Shuttleworth-Wallace, and
782 modified Priestley-Taylor evapotranspiration models for wildland vegetation in
783 semiarid rangeland, Water Resour. Res., 29, 1379-1392, 1993.

784 Tahiri, A. Z., Anyoji, H., and Yasuda, H.: Fixed and variable light extinction
785 coefficients for estimating plant transpiration and soil evaporation under irrigated
786 maize, Agr. Water Manage., 84, 186-192, 2006.

787 Teuling, A. J., Uijlenhoet, R., Hupert, F., and Troch, P. A.: Impact of plant water
788 uptake strategy on soil moisture and evapotranspiration dynamics during drydown,
789 Geophys. Res. Lett., 33, L03401, doi:10.1029/2005GL025019, 2006.

790 Thomas, H., and Sansom, M.: Fully coupled analysis of heat, moisture, and air
791 transfer in unsaturated soil, J. Eng. Mech.-ASCE, 121, 392-405, 1995.

792 Van De Griend, A. A., and Owe, M.: Bare soil surface resistance to evaporation by
793 vapor diffusion under semiarid conditions, Water Resour. Res, 30, 181-188, 1994.

794 Van Genuchten, M. T.: A closed-form equation for predicting the hydraulic
795 conductivity of unsaturated soils, Soil Sci. Soc. Am. J., 44, 892-898, 1980.

796 Verma, P., Loheide, S. P., Eamus, D., and Daly, E.: Root water compensation sustains
797 transpiration rates in an Australian woodland, Adv. Water. Resour., 74, 91-101,
798 2014.

799 Vörösmarty, C. J., Federer, C. A., and Schloss, A. L.: Potential evaporation functions
800 compared on US watersheds: Possible implications for global-scale water balance
801 and terrestrial ecosystem modeling, J. Hydrol., 207, 147-169, 1998.

802 Wang, J., Cai, H., Kang, Y., and Chen, F.: Ratio of soil evaporation to the
803 evapotranspiration for summer maize field, Nongye Gongcheng Xuebao/T. Chinese
804 Soc. Agr. Eng., 23, 17-22, 2007.

805 Wang, W., Wang, Q., and Fan, J.: Relationship between air permeability, water
806 conductivity and water content for undisturbed and disturbed soils, Nongye
807 Gongcheng Xuebao/ T. Chinese Soc. Agr. Eng., 24, 25-29, 2008.

808 Wei, Z., Paredes, P., Liu, Y., Chi, W. W., and Pereira, L. S.: Modelling transpiration,
809 soil evaporation and yield prediction of soybean in North China Plain, Agr. Water
810 Manage., 147, 43-53, 2015.

811 Willmott, C. J.: On the validation of models, Phys. Geogr., 2, 184-194, 1981.

812 Willmott, C. J., Ackleson, S. G., Davis, R. E., Feddema, J. J., Klink, K. M., Legates,
813 D. R., O'donnell, J., and Rowe, C. M.: Statistics for the evaluation and comparison
814 of models, J. Geophys. Res.-Oceans, 90, 8995-9005, 1985.

815 Wu, J., Zhang, R., and Gui, S.: Modeling soil water movement with water uptake by
816 roots, Plant Soil, 215, 7-17, 1999.

817 Zeng, Y., Su, Z., Wan, L., Yang, Z., Zhang, T., Tian, H., Shi, X., Wang, X., and Cao,
818 W.: Diurnal pattern of the drying front in desert and its application for determining

819 the effective infiltration, Hydrol. Earth Syst. Sci., 13, 703-714,
820 doi:10.5194/hess-13-703-2009, 2009a.

821 Zeng, Y., Wan, L., Su, Z., Saito, H., Huang, K., and Wang, X.: Diurnal soil water
822 dynamics in the shallow vadose zone (field site of China University of Geosciences,
823 China), Environ. Geol., 58, 11-23, 2009b.

824 Zeng, Y., Su, Z., Wan, L., and Wen, J.: Numerical analysis of air-water-heat flow in
825 unsaturated soil: Is it necessary to consider airflow in land surface models?, J.
826 Geophys. Res.-Atmos., 116, D20107, doi:10.1029/2011JD015835, 2011a.

827 Zeng, Y., Su, Z., Wan, L., and Wen, J.: A simulation analysis of the advective effect
828 on evaporation using a two-phase heat and mass flow model, Water Resour. Res.,
829 47, W10529, doi:10.1029/2011WR010701, 2011b.

830 Zhang, B., Liu, Y., Xu, D., Cai, J., and Zhao, N.: Estimation of summer corn canopy
831 conductance by scaling up leaf stomatal conductance, Nongye Gongcheng Xuebao/
832 T. Chinese Soc. Agr. Eng., 27, 80-86, 2011.

833 Zhao, N., Liu, Y., Cai, J., Paredes, P., Rosa, R. D., and Pereira, L. S.: Dual crop
834 coefficient modelling applied to the winter wheat–summer maize crop sequence in
835 North China Plain: Basal crop coefficients and soil evaporation component, Agr.
836 Water Manage., 117, 93-105, 2013.

837 Zhou, M. C., Ishidaira, H., Hapuarachchi, H. P., Magome, J., Kiem, A. S., and
838 Takeuchi, K.: Estimating potential evapotranspiration using Shuttleworth-Wallace
839 model and NOAA-AVHRR NDVI data to feed a distributed hydrological model
840 over the Mekong River basin, J. Hydrol., 327, 151-173, 2006.

841 Zhou, M. C., Ishidaira, H., and Takeuchi, K.: Estimation of potential
842 evapotranspiration over the Yellow River basin: Reference crop evaporation or
843 Shuttleworth-Wallace?, Hydrol. Process., 21, 1860-1874, 2007.

844

845

Tables and Figures

Table 1. Crop growth stages and crop height for maize

Crop growth stages		Date	Crop height (m)
Initial	Start	23/06 (DOY 174)	0
Crop development	Start	06/07 (DOY 187)	0.22
Mid-season	Start	14/08 (DOY 226)	1.65
Late season	Start	14/09 (DOY 257)	2.17
	Harvest	02/10 (DOY 275)	2.17

DOY, day of the year

849 **Table 2.** Soil hydraulic (Van Genuchten, 1980) and thermal (De Vries, 1963)
850 properties including saturated (θ_s) and residual (θ_r) water content; curve-fitting
851 parameters (α and n); saturated hydraulic conductivity (K_s); specific heat capacities of
852 the water (C_w), air (C_a), quartz (C_q), clay (C_c) and organic matter (C_o)

Soil sample	Hydraulic properties					Thermal properties				
	θ_s	θ_r	α	n	K_s	C_w	C_a	C_q	C_c	C_o
	$cm^3\ cm^{-3}$		cm^{-1}	/	$cm\ d^{-1}$	$J\ g^{-1}\ K^{-1}$				
0-20cm	0.45	0.105	0.0045	1.41	10.50	4.18	1.01	0.80	0.90	1.92

853

854 **Table 3.** Statistical summary of the correlation between observed and simulated
855 hourly ET for each crop development stage, for both the ET_{dir} method and the ET_{ind}
856 method.

Crop stage	Number of observations	ET_{ind} method					ET_{dir} method				
		a	b	R^2	RMSE (mm h^{-1})	d	a	b	R^2	RMSE (mm h^{-1})	d
Initial	336	0.47	0.054	0.40	0.10	0.84	0.94	0.043	0.63	0.10	0.90
Crop development	936	0.69	0.064	0.70	0.10	0.94	0.81	0.041	0.78	0.09	0.96
Mid-season	744	0.62	0.055	0.80	0.11	0.93	0.89	0.027	0.90	0.08	0.98
Late season	432	0.70	0.051	0.72	0.07	0.90	0.75	0.029	0.77	0.06	0.93
Total season	2448	0.65	0.056	0.72	0.11	0.90	0.85	0.035	0.82	0.09	0.95

857 *the regression relation is $ET_{sim} = a \times ET_{obs} + b$; a is the slope and b is the intercept.

858 **Table 4.** Evaporation (E), transpiration (T_c), evapotranspiration (ET) and evaporation
859 fraction (E/ET, EF) for each development stage of maize, for both the ET_{dir} method
860 and the ET_{ind} method. The actual evapotranspiration (ETc) is shown as well.

Crop stage	ETc (mm)	ET_{ind} method				ET_{dir} method			
		E (mm)	T (mm)	ET (mm)	EF (%)	E (mm)	T (mm)	ET (mm)	EF (%)
Initial	37.72	29.13	6.83	35.96	81.01	43.32	6.71	50.03	86.58
Crop development	140.48	34.57	122.73	157.31	21.98	45.17	107.13	152.30	29.66
Mid-season	124.74	12.15	105.75	117.91	10.31	32.01	99.26	131.26	24.38
Late season	31.23	9.50	34.22	43.72	21.73	14.10	21.66	35.77	39.43
Total season	334.18	85.36	269.53	354.89	24.05	134.60	234.76	369.37	36.44

861

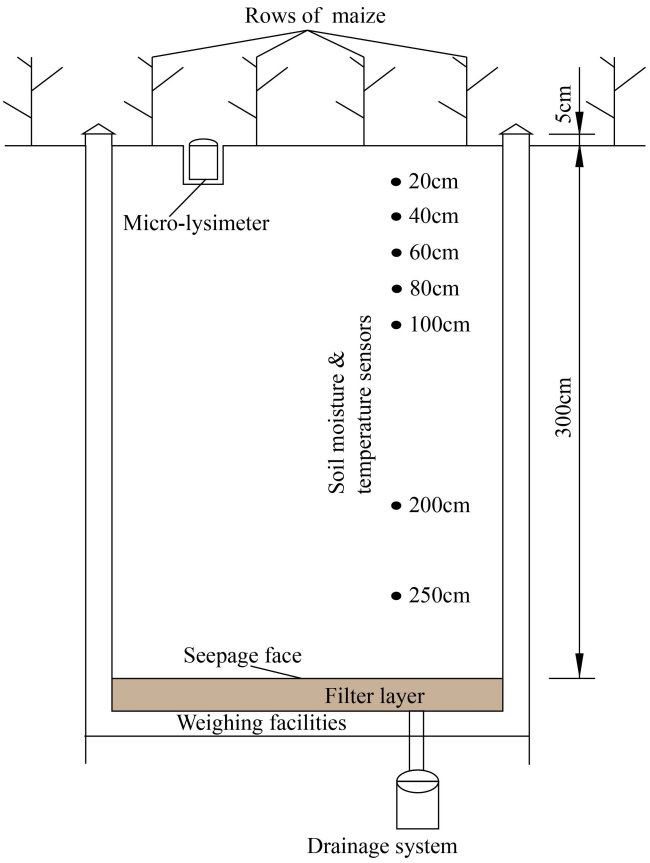

862 **Figure 1.** Schematic drawing of the large lysimeter structure

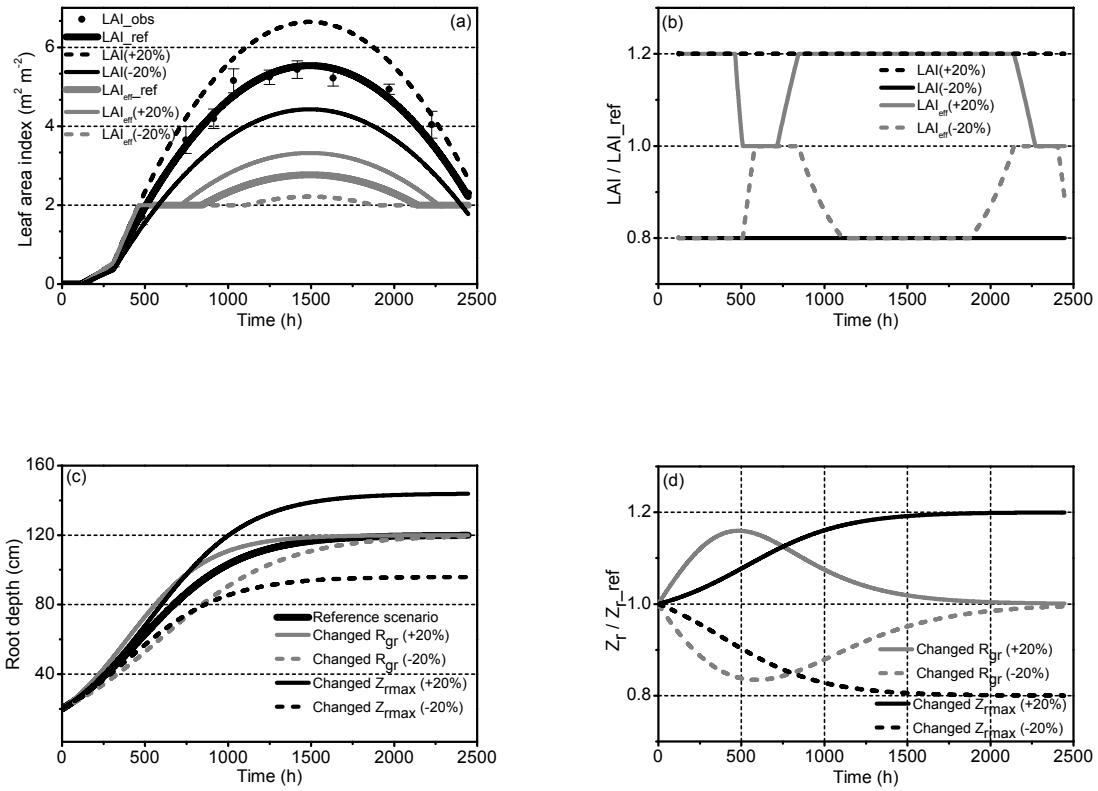

Figure 2. The seasonal variation in crop growth parameters used in the simulations: (a) leaf area index (LAI), (b) relative values of LAI compared to the reference scenario, (c) root depth (Z_r), and (d) relative values of root depth compared to the reference scenario. +20% and -20% indicate a 20% increase or decrease, respectively, compared to the reference value. The vertical gridlines in (d) highlight the lag effect of the 20% decreased R_{gr} scenario compared to the 20% increased R_{gr} scenario.

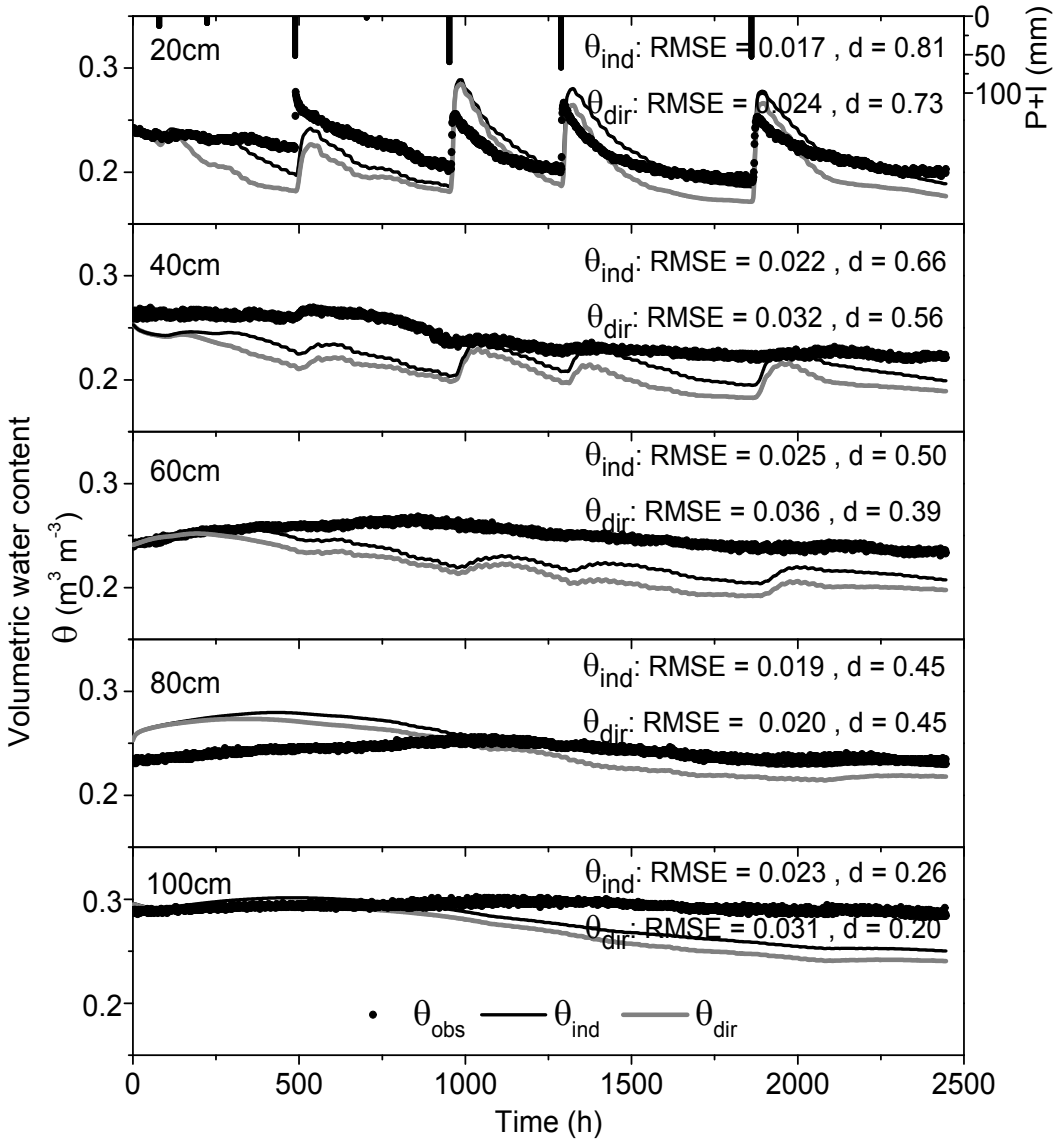

872

873 **Figure 3.** Comparison of observed and simulated soil volumetric water content, at
874 selected depths: 20cm, 40cm, 60cm, 80cm and 100cm, with measured precipitation
875 and irrigation (the solid black bar with the right axis of "P+I (mm)"). The (connected)
876 black dots represent measurements, the black line depicts the simulation using the
877 ET_{ind} method, and the gray line depicts the simulation using the ET_{dir} method.

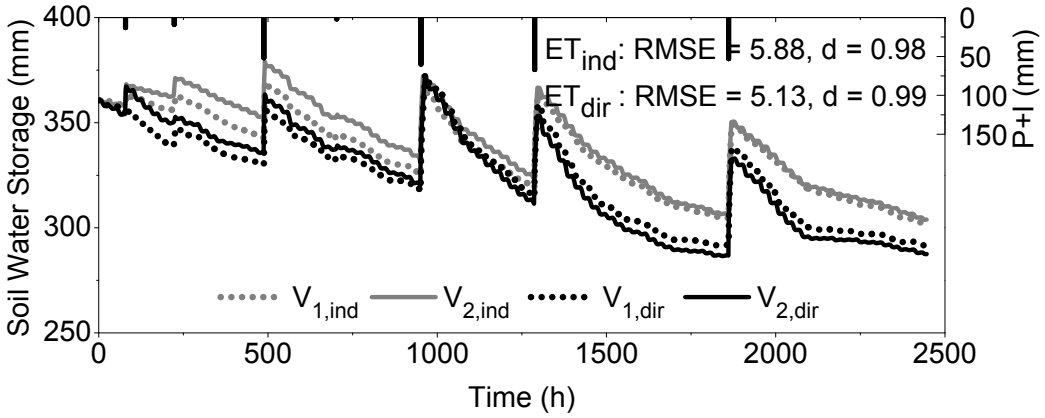

878
879

880 **Figure 4.** Comparison between simulated root-zone water storage using different
881 methods (i.e. $V_{1,ind}$, $V_{2,ind}$, $V_{1,dir}$, $V_{2,dir}$), with measured precipitation and irrigation. The
882 grey dotted line represents water storage calculated with the integration of soil water
883 content over the root-zone and the grey solid line represents water storage calculated
884 with the inversion of the water balance equation within the root-zone, using the ET_{ind}
885 method, i.e. $V_{1,ind}$, $V_{2,ind}$, respectively. The black dotted and solid lines represent the
886 ET_{dir} method.

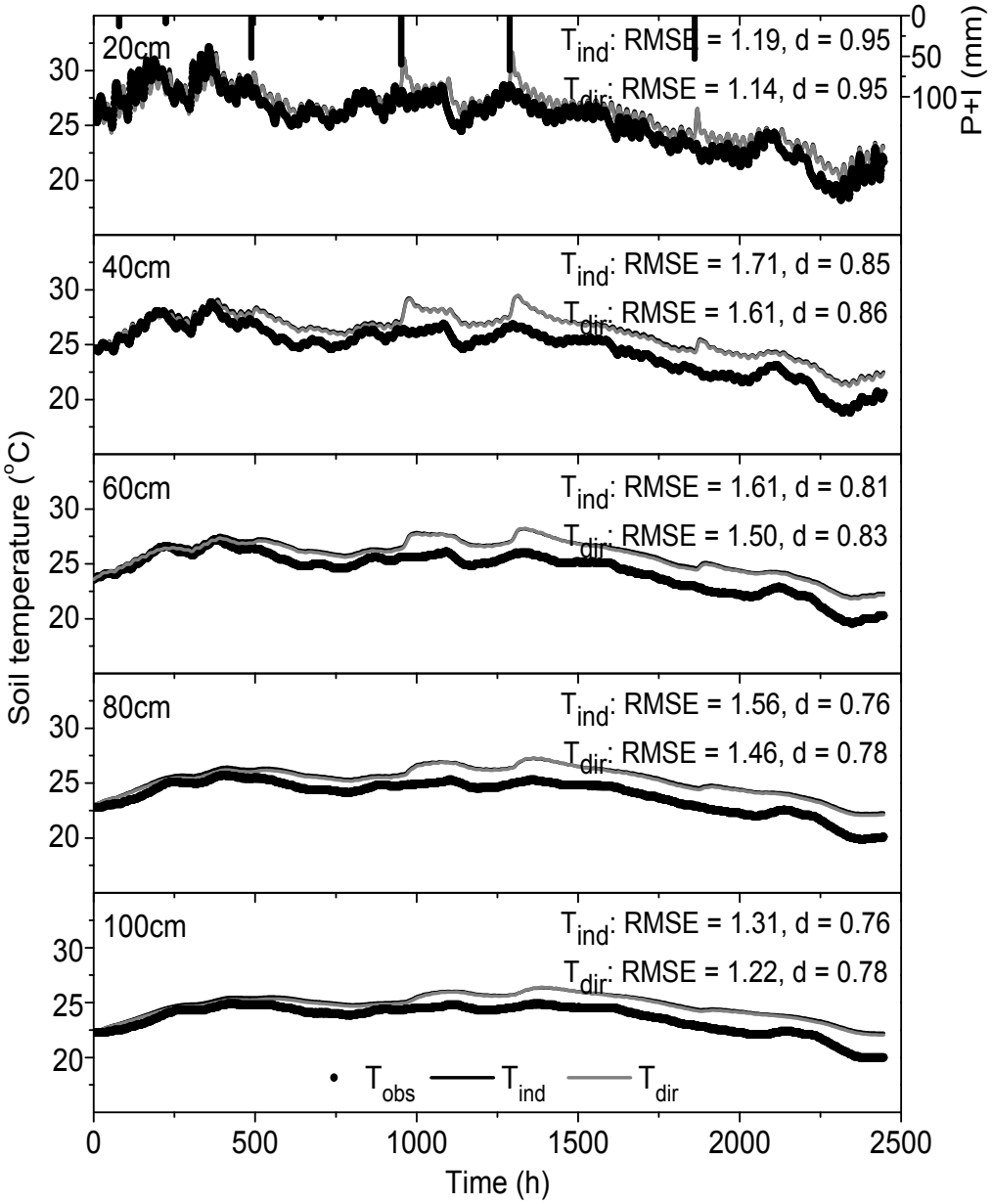

887

888 **Figure 5.** Comparison of observed and simulated soil temperature, at selected depths:
889 20cm, 40cm, 60cm, 80cm and 100cm, with measured precipitation and irrigation. The
890 black dots represent the observation, the solid black line shows the simulation with
891 the ET_{ind} method, and the solid gray line shows the simulations with the ET_{dir} method.

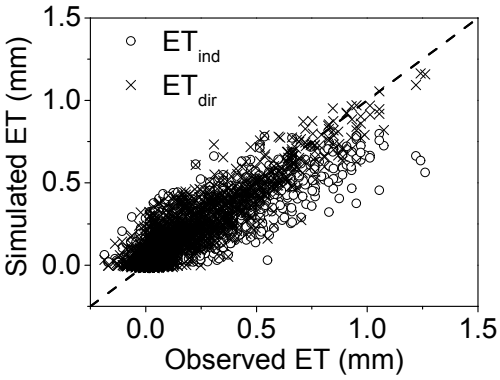

892

893 **Figure 6.** Scatter plot of hourly observed and simulated ET rates, with × being
894 estimations using the ET_{dir} method and ○ being estimations using the ET_{ind} method.

895

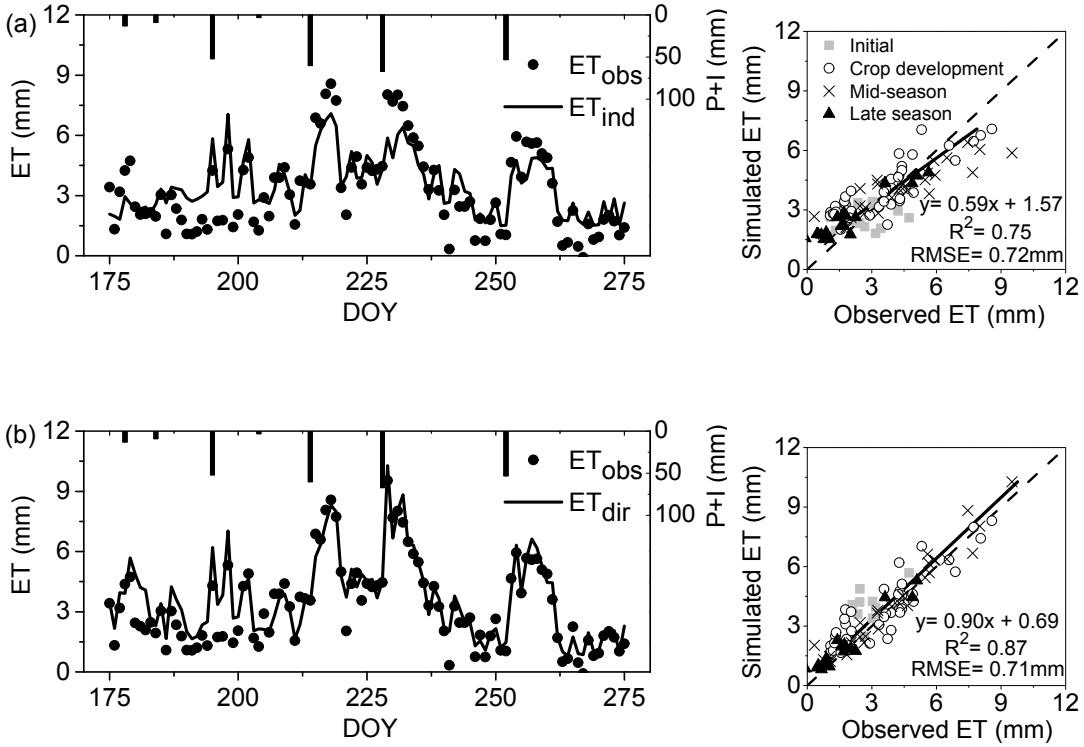

Figure 7. Daily variation in observed ET and simulated ET, based on the ET_{ind} method (a) and the ET_{dir} method (b). On the right: the regression between observed and simulated ET for the ET_{ind} method (above) and the ET_{dir} method (below).

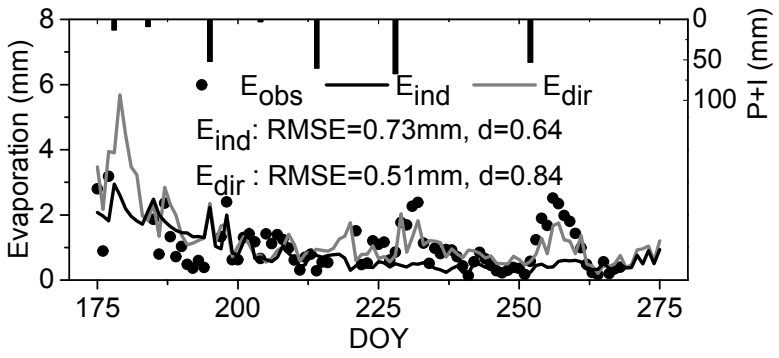

901

902 **Figure 8.** Daily variation in observed and simulated soil evaporation based on the two

903 ET simulation methods.

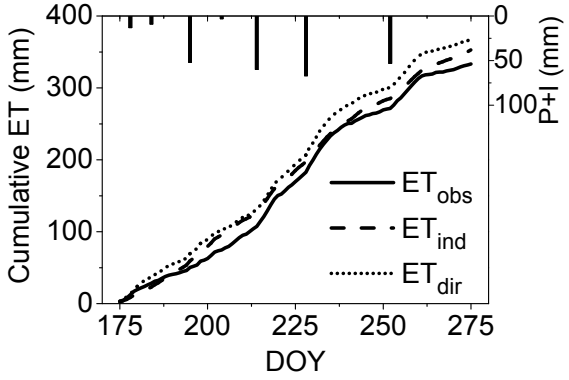

904

905 **Figure 9.** Cumulative variation in observed ET and simulated ET (as deducted from
906 the two ET simulation methods).

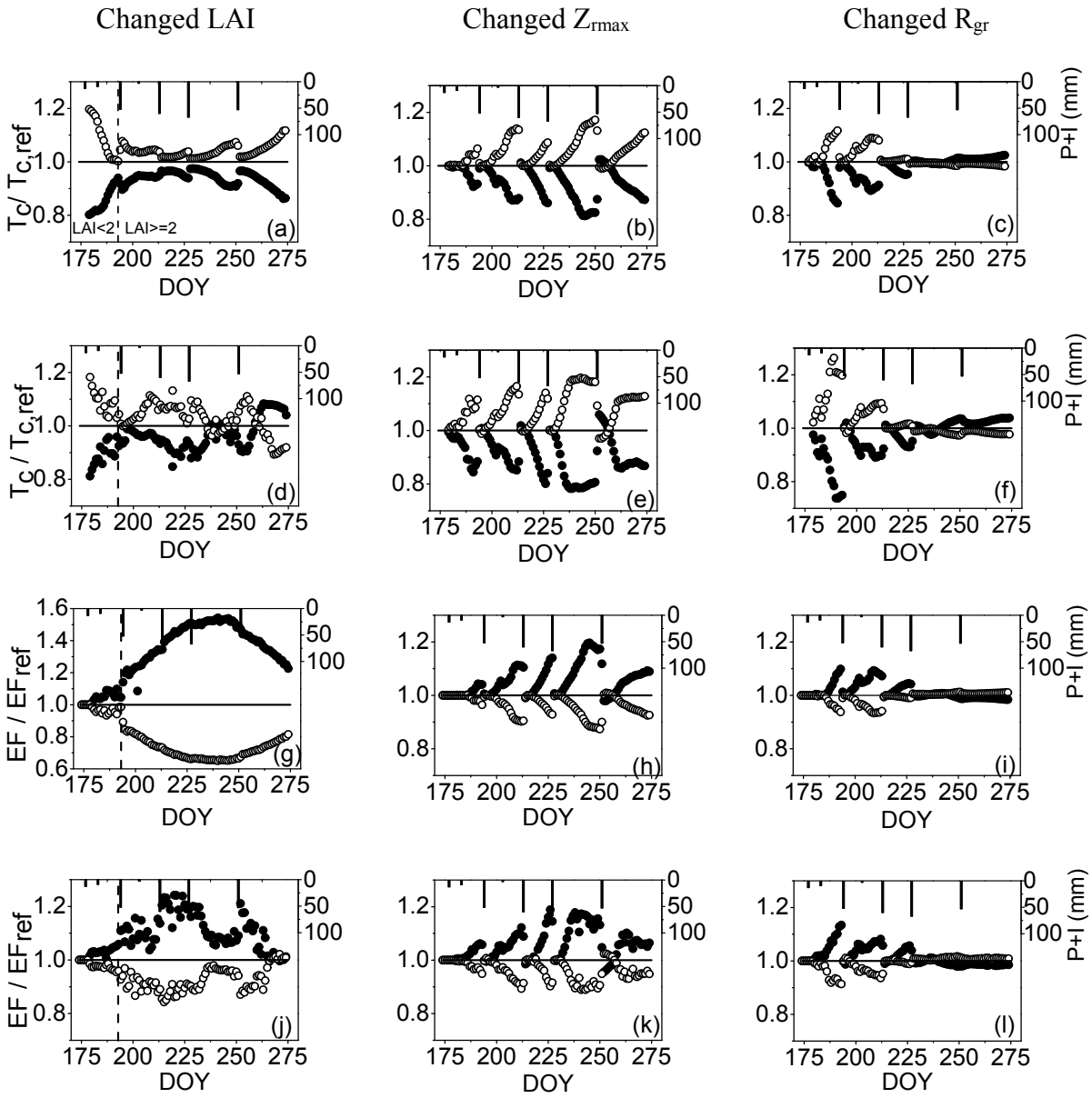

907

908 **Figure 10.** Relative daily variations, under changed leaf area index (LAI), maximum
909 rooting depth (Z_{rmax}) and root growth rate (R_{gr}), in crop transpiration: (a)-(c), using the
910 ET_{ind} method, (d)-(f), using the ET_{dir} method; and in the evaporation fraction: (g)-(i),
911 using the ET_{ind} method; (j)-(l), using the ET_{dir} method, with measured precipitation
912 and irrigation; ○ depicting increased LAI, Z_{rmax} and R_{gr} by 20%, ● depicting
913 decreased LAI, Z_{rmax} and R_{gr} by 20%. Note that scale for (*g*) differs from for other
914 figures.

915